



Résolution sismique latérale le long d'une interface courbe entre deux milieux anisotropes : cas des ondes réfléchies

N. Favretto-Cristini^a, B. Ursin^b et P. Cristini^a

^aCNRS, Laboratoire de Mécanique et d'Acoustique UPR 7051, 31 chemin Joseph-Aiguier, 13402
Marseille, France

^bNTNU -Department of Petroleum Engineering and Applied Geophysics, S.P. Andersens vei 15A, N-7491
Trondheim, Norvège
favretto@lma.cnrs-mrs.fr

The Fresnel volume and the Interface Fresnel Zone (IFZ) concepts play an important role in seismic exploration, as the IFZ largely contributes to the formation of the reflection and transmission wavefields at an observation point. We derive analytical expressions for the IFZ size for (possibly converted) waves reflected by a curved interface between dip-constrained transversely isotropic media. The reflectors are of anticline, syncline, or saddle type, and their principal curvatures axes may not lie in the incidence plane. As in an anisotropic medium the isochron assumes, in most cases, a non-elliptical shape, the size and the shape of the IFZ for reflected waves are predominantly dependent on the curvatures of the isochrons together with the curvatures of the interface. The IFZ shapes also exhibit large variation with interface curvature and incidence angle. In addition, the difference between the anisotropic Thomsen parameters ϵ and δ is found to control the size of the IFZ for both P-P and P-S reflections. Numerical illustrations for P-P reflections show that the IFZ for anisotropic media can be much larger than that for equivalent isotropic media, more specifically for positive values of $\epsilon - \delta$. The spatial resolution of unmigrated seismic data in anisotropic media would consequently be different from that determined for the same configuration if the media were assumed to be isotropic and the interface plane.

1 Introduction

The Interface Fresnel Zone (IFZ) concept plays an important role in seismic exploration, as the IFZ largely contributes to the formation of the reflection and transmission wavefields at an observation point. This finite area of a reflector can be viewed as the region of constructive reflection interference surrounding the reflection point of the geometrical ray. The IFZ determines the spatial resolving power for unmigrated seismic data with which important lithological changes along a seismic profile direction may be observed. Additionally, it also largely contributes to the reflected and transmitted wavefields, and more specifically to their amplitude [12, 5, 6]. As a consequence, the IFZ has received increasing attention in past decades, and analytical and numerical modeling techniques have been used to determine the IFZ dimensions in various configurations [9, 4, 11, 2, 8, 10, 7]. Most studies, however, have been concerned with zero-offset configurations and plane reflectors and few works have been devoted to anisotropic media and curved reflectors. Here we present simple analytical expressions for the IFZ for multi-offset configurations and a curved interface between dip-constrained transversely isotropic (DTI) media. We generalize the relationships given in [7] for (possibly converted) reflected waves from a reflector of anticline-, syncline-, or saddle-type whose principal curvature axes may not lie in the incidence plane.

2 Interface Fresnel Zone for reflections in DTI media

We consider a curved interface between two homogeneous DTI media. The symmetry axis of each medium being parallel to the interface normal at each point of the interface, the DTI media are VTI media with respect to the local coordinate system at the reflection point. An incident wave strikes the interface and gives rise to reflected waves and transmitted waves. The three wave types which may occur are the SH-wave and the coupled P-SV waves. The x_1 -axis lies in the surface tangent plane and in the plane defined by the surface normal (along the x_3 -axis) and the slowness of the incident wave (Figure 1). Because of the symmetry all seismic signatures depend only on the angle between the propagation direction and the symmetry axis. The slownesses of the incident and reflected waves lie then all in the $x_1 - x_3$ plane, *i.e.* the plane of incidence. This implies

that the out-of-plane components of the group velocity vector \mathbf{V} and slowness vector \mathbf{p} are equal to zero in all cases. From the relation $\mathbf{x} = \frac{d}{V} \mathbf{V}$ we note that x_2 is equal to zero as well. The superscript S denotes the quantities for the incident wave, and R for the reflected wave.

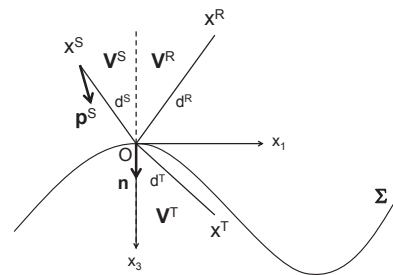


Figure 1: Incident, reflected and transmitted waves at a curved interface Σ between two anisotropic media

The Fresnel volumes (FV) associated with the reflected or transmitted wave are defined by

$$\left| \delta T(\mathbf{x}^S, \delta \mathbf{x}) + \delta T(\mathbf{x}^U, \delta \mathbf{x}) \right| \leq \frac{1}{2f} \quad (U = R, T) \quad (1)$$

where f is the dominant frequency of the signal. The difference in traveltime δT , between a ray from a point x to the origin O (*i.e.*, $T(\mathbf{x}, 0)$) and from the point x to a point at δx near the origin O (*i.e.*, $T(\mathbf{x}, \delta \mathbf{x})$), has to be replaced with its approximation

$$\delta T(\mathbf{x}, \delta \mathbf{x}) \approx \frac{1}{2Vd} \left[\|\delta \mathbf{x}\|^2 - 2\mathbf{x} \cdot \delta \mathbf{x} - \left(\frac{\mathbf{x} \cdot \delta \mathbf{x}}{d} \right)^2 \right] \quad (2)$$

with appropriate superscript, where $V = \|\mathbf{V}\| = (V_1^2 + V_2^2 + V_3^2)^{\frac{1}{2}}$ is the group velocity, and $d = \|\mathbf{x}\|$. In Eq. 2 we have neglected changes in group velocity (*i.e.*, $\frac{\delta V}{V} \ll 1$).

The wave is reflected or transmitted at a curved interface Σ which may locally be approximated by a second-order expression

$$x_3 = F(x_1, x_2) = \frac{1}{2} (x_1, x_2) \mathbf{F} (x_1, x_2)^t \quad (3)$$

where F defines the interface parameters. For the Fresnel zones at the curved interface we have $\delta x_3 = F(\delta x_1, \delta x_2)$.

The IFZ for the reflected wave is defined as the points on the curved interface Σ which satisfy the inequality

$$\left| \delta T_{\Sigma}(\mathbf{x}^S, \delta x_1, \delta x_2) + \delta T_{\Sigma}(\mathbf{x}^R, \delta x_1, \delta x_2) \right| \leq \frac{1}{2f} \quad (4)$$

In Eq. 4 the difference in traveltimes δT_{Σ} between the source (respectively, the receiver) and the reflection point has to be replaced with its approximation with appropriate superscript (S or R):

$$\delta T_{\Sigma}(\mathbf{x}, \delta x_1, \delta x_2) \simeq \frac{1}{2Vd} \left[\left(1 - \frac{x_1^2}{d^2} \right) \delta x_1^2 + \delta x_2^2 - 2x_1 \delta x_1 - 2F(\delta x_1, \delta x_2) x_3 \right] \quad (5)$$

where $d = [(x_1)^2 + (x_3)^2]^{\frac{1}{2}}$ and $V = (V_1^2 + V_3^2)^{\frac{1}{2}}$ with [3]

$$\begin{cases} V_1 = p_1 \frac{a_{11} B_2 + a_{44} B_1 - p_3^2 A^2}{B_1 + B_2} \\ V_3 = p_3 \frac{a_{44} B_2 + a_{33} B_1 - p_1^2 A^2}{B_1 + B_2} \end{cases} \quad (6)$$

where, for a given horizontal slowness p_1 ,

$$p_3^2 = \frac{B \mp [B^2 - 4a_{33} a_{44} (a_{11} p_1^2 - 1) (a_{44} p_1^2 - 1)]^{1/2}}{2a_{33} a_{44}} \quad (7)$$

with $B = a_{33} + a_{44} + (a_{13}^2 + 2a_{13} a_{44} - a_{11} a_{33}) p_1^2$, $B_1 = a_{11} p_1^2 + a_{44} p_3^2 - 1$ and $B_2 = a_{44} p_1^2 + a_{33} p_3^2 - 1$, and where $a_{ij} = c_{ij}/\rho$ are the density-normalized elastic constants in Voigt notation. In Eq. 7 the minus sign is for the P wave, and the plus sign is for the SV wave. Remember that \mathbf{x} and \mathbf{V} are connected through $\mathbf{x} = \frac{d}{V} \mathbf{V}$.

Relations 6 are exact expressions for the group velocity components. Even if it is preferable to use them in actual modeling, inversion and processing algorithms, we can use instead the approximate relations, valid for media with weak anisotropy, in order to gain valuable analytic insight into the effects of anisotropy on the IFZ :

$$\begin{cases} V_{P1} = v_{P0}^2 p_1 [(1 + 2\epsilon) - 2(\epsilon - \delta) \chi] \\ V_{P3} = v_{P0}^2 p_3 [1 - 2(\epsilon - \delta) \chi'] \end{cases} \quad (8)$$

$$\begin{cases} V_{S1} = v_{S0}^2 p_1 [1 + 2\sigma \chi] \\ V_{S3} = v_{S0}^2 p_3 [1 + 2\sigma \chi'] \end{cases} \quad (9)$$

with

$$\begin{cases} \chi = \frac{p_3^4}{(p_3^2 + \xi p_1^2)^2} \\ \chi' = \frac{\xi p_1^4}{(p_3^2 + \xi p_1^2)^2} \end{cases} \quad (10)$$

and

$$\sigma = \frac{v_{P0}^2}{v_{S0}^2} (\epsilon - \delta) \quad (11)$$

$$\xi = 1 + 2\epsilon \frac{v_{P0}^2}{v_{P0}^2 - v_{S0}^2} \quad (12)$$

where the notation of [14] is used

$$\begin{cases} v_{P0} = \left(\frac{c_{33}}{\rho} \right)^{1/2} \\ v_{S0} = \left(\frac{c_{44}}{\rho} \right)^{1/2} \\ \epsilon = \frac{c_{11} - c_{33}}{2c_{33}} \\ \delta = \frac{(c_{13} + c_{44})^2 - (c_{33} - c_{44})^2}{2c_{33}(c_{33} - c_{44})} \end{cases} \quad (13)$$

v_{P0} and v_{S0} are the vertical velocities defined from the medium density ρ and the elastic constants c_{ij} given in Voigt notation.

From Eqs 5, 8 and 9 we note that besides the interface parameters F and the vertical velocities v_{P0} and v_{S0} , the difference $\epsilon - \delta$ also controls the shape and the size of the IFZ for both P-P and P-SV reflections.

3 Numerical examples

Here the shape and the size of the IFZ for P-P reflections are investigated for various anisotropic parameters, incidence angles, and interface curvatures. The purpose is to demonstrate how all these parameters, and specifically the anisotropic parameters, may control the IFZ size and hence the lateral seismic resolution. In order to emphasize this influence, we compare the results with those obtained for the equivalent isotropic media and plane reflectors.

3.1 Description of the model

We use the measured values of anisotropic parameters in brine-saturated shales [16]. The incidence medium has density $\rho = 2597 \text{ kg/m}^3$, vertical P-wave velocity $v_{P0} = 4409 \text{ m/s}$, vertical S-wave velocity $v_{S0} = 2688 \text{ m/s}$, and dimensionless anisotropic (Thomsen) parameters $\epsilon = 0.110$ and $\delta = -0.043$. Velocities and Thomsen parameters are connected to elastic coefficients $a_{ij} = c_{ij}/\rho$ [15]. Hereafter we will consider more specifically the difference $\epsilon - \delta$ which is known to primarily govern P-wave signatures [15] and which seems to also control the IFZ size for both P-P and P-SV reflections. The difference $\epsilon - \delta$ has a positive value ($\epsilon - \delta = 0.153$) for real brine-saturated shales. For comparison purpose, and in order to emphasize the influence of this difference on the shape and the size of the IFZ, we fix the values for ρ , v_{P0} , and v_{S0} , and we also consider a negative value for $\epsilon - \delta$ (-0.153). The source and the receiver are located at a distance $x_3 = 3000 \text{ m}$ from the plane tangent to the interface at the reflection point. The prevailing frequency f of the incident P-wave is chosen equal to 25 Hz . The incident P-wavelength at normal incidence is then 176 m .

We consider three kinds of curved reflector in this study: an anticline-type reflector with positive values for the main radii of interface curvature ($R_1 = +5000 \text{ m}$ and $R_2 = +4000 \text{ m}$), a syncline-type reflector with negative values for radii ($R_1 = -5000 \text{ m}$ and $R_2 = -4000 \text{ m}$), and a saddle-type reflector with $R_1 = -5000 \text{ m}$ and $R_2 = +4000 \text{ m}$. To remain general we cannot suppose that δx_1 and δx_2 lie along the principal curvature axes of the interface, as the x_1 -direction is given by the incoming ray, which implies that the functions F_{ij} ($i, j = 1, 2$) in Eq. 3 can be expressed as [13]

$$\begin{cases} F_{11} = \frac{1}{R_1} \cos^2 \phi + \frac{1}{R_2} \sin^2 \phi \\ F_{12} = \left(\frac{1}{R_1} - \frac{1}{R_2} \right) \cos \phi \sin \phi \\ F_{22} = \frac{1}{R_1} \sin^2 \phi + \frac{1}{R_2} \cos^2 \phi \end{cases} \quad (14)$$

where ϕ is the angle between the principal curvature axes of the interface and the Cartesian coordinate axes. Hereafter we will consider $\phi = 20^\circ$. We also consider the particular case where δx_1 and δx_2 both lie along the principal curvature axes of the interface, which implies $\phi = 0$, and hence

$$\begin{cases} F_{11} = \frac{1}{R_1} \\ F_{12} = 0 \\ F_{22} = \frac{1}{R_2} \end{cases} \quad (15)$$

Note that for a plane reflector the radii R_1 and R_2 have infinite values.

3.2 Influence of $\epsilon - \delta$ on the IFZ for P-P reflection from various curved reflectors

We study the effects of the difference $\epsilon - \delta$ on the shape and the size of the IFZ for P-P reflection for various incidence angles and various interface curvatures.

Figure 2 illustrates the results for a plane reflector. For comparison purposes we also show the IFZs for the equivalent isotropic medium ($\epsilon = \delta = 0$). The size of each IFZ is normalized with respect to the incident P-wavelength for $\theta = 0$. For $\theta = 0$ the anisotropic IFZ is equivalent to the isotropic counterpart and exhibits circular shape. This striking result seems to be conflicting with that presented in [11]. In fact, our zero-offset results for anisotropic media are due to the traveltimes approximation which consists in an expansion in a Taylor series around the central ray. Since the reflector dip is zero, the zero-offset rays depend only on the vertical velocity of the medium, and the results are the same as for isotropic media. Nevertheless, with increasing θ the anisotropic IFZ shows significant changes in shape with respect to the isotropic counterpart. These changes are much more pronounced for positive values of $\epsilon - \delta$.

Figures 3, 4 and 5 present the variation in shape and size of the IFZ at an anticline-, syncline-, and saddle-type reflector, respectively, as a function of $\epsilon - \delta$ and for various incidence angles θ . The principal curvature axes of the reflectors lie along the Cartesian coordinate axes.

As expected in the case of an anticline, since a smaller area of the interface is in contact with the isochron, the anisotropic IFZ is smaller than that at the plane reflector. Whatever the value for $\epsilon - \delta$ and for small (or moderate) incidence angles, the size and the shape of the anisotropic IFZ are quite identical to the isotropic counterparts (Figure 3).

On the contrary, the anisotropic IFZ at the syncline-type reflector exhibits a more complex shape with increasing θ (Figure 4). For small incidence angles the IFZ has an elliptical shape with the major axis lying in the transverse plane, whatever the value for $\epsilon - \delta$. As the angle θ increases the curvature of the isochron tends to that of the reflector over a very large distance, which leads to growing portions of the reflectors involved in the reflection process, and hence an unusually large IFZ in the incidence plane (*e.g.*, for $\theta = 35^\circ$ in Figure 4). Whatever the value for $\epsilon - \delta$, the size of the anisotropic IFZ at a syncline is larger than the isotropic counterpart. Nevertheless, this feature is still more pronounced for positive values of $\epsilon - \delta$. Note that for wider incidence angles the anisotropic IFZ exhibits four infinitely extended tails along diagonal directions, known as indicators of the existence of stationary points of hyperbolic type [1, 12]. Nevertheless, these tails are devoid of physical sense and must be truncated to obtain the actual field-formation region which is of finite size [1]. The real size of the anisotropic IFZ is then given by the ellipse tangent to the vertices of hyperbolae and whose axes lie in the incidence and transverse planes.

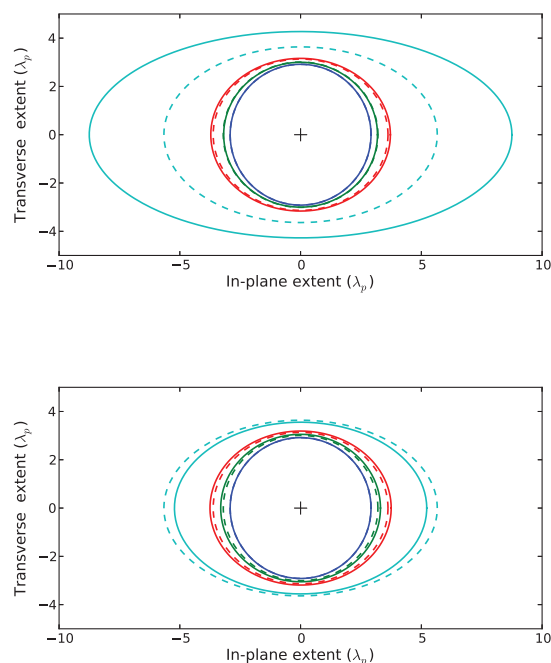


Figure 2: Variation in shape and size of the IFZ for P-P reflection from a plane reflector between anisotropic (solid line) and isotropic (dashed line) media, as a function of the difference $\epsilon - \delta$ (with positive (top) or negative (bottom) value) and for various incidence angles θ . The incidence angles are $\theta = 0$ (dark blue), $\theta = 20^\circ$ (green), $\theta = 30^\circ$ (red), and $\theta = 50^\circ$ (light blue).

The anisotropic IFZ at the saddle-type reflector exhibits a specific shape which is a mix between the shapes of the anisotropic IFZ at the anticline and at the syncline (Figure 5). As expected from the values of the main radii of the interface curvature, its size is limited in the incidence (respectively, transverse) plane by the extent of the anisotropic IFZ at the syncline (respectively, anticline). The anisotropic IFZ at the saddle-type reflector is larger than the isotropic counterpart, this feature still being more pronounced for positive values of $\epsilon - \delta$.

Considering the general case where the principal curvature axes of the reflectors do not lie along the Cartesian coordinate axes leads to no minor changes in the shape and the size of the IFZ for anticline-type reflector (Figure 6). The changes however are significant for syncline- and saddle-type reflectors (Figures 7 and 8). The IFZ patterns still remain ellipses expanding from the fixed reflection point with increasing incidence angle, but they are now rotated by the angle $\phi = 20^\circ$ with respect to the x_1 -axis. In addition to the rotation of the patterns, the rotation of the principal curvature axes of the reflectors leads to larger (respectively, smaller) size of the isotropic and anisotropic IFZs at the syncline (respectively, saddle-type reflector) along the direction of the principal curvature axis associated with radius R_1 , the size along the perpendicular direction remaining unchanged. Moreover, the occurrence of the infinitely extended tails along diagonal directions can be noted at the syncline for smaller incidence angles than

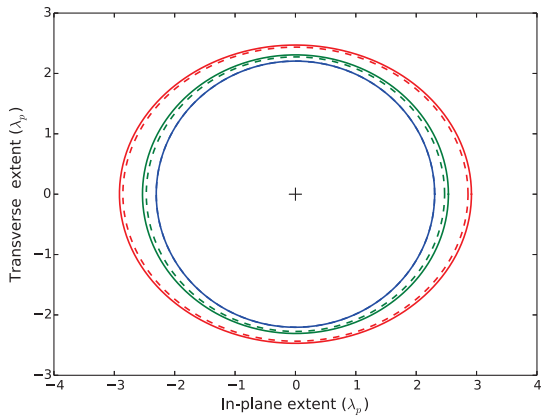
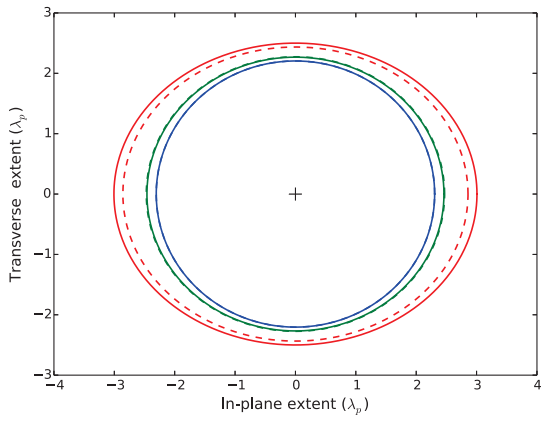


Figure 3: Variation in shape and size of the IFZ for P-P reflection in anisotropic (solid line) and isotropic (dashed line) media at an anticline-type reflector, as a function of the difference $\epsilon - \delta$ with positive (top) and negative (bottom) value and for various incidence angles θ . The incidence angles are $\theta = 0$ (dark blue), $\theta = 20^\circ$ (green), and $\theta = 35^\circ$ (red). The principal curvature axes of the reflectors lie along the Cartesian coordinate axes.

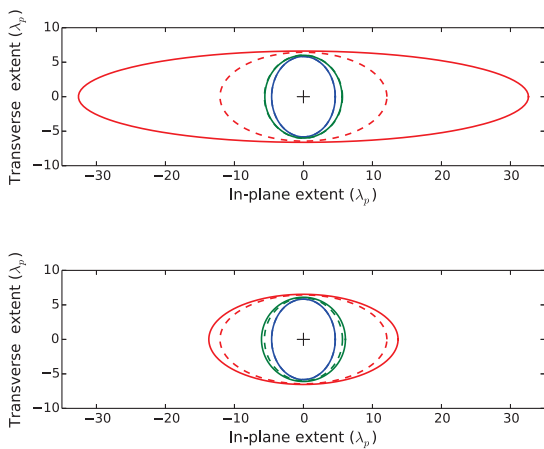


Figure 4: Same as in Figure 3, but for a syncline-type reflector.

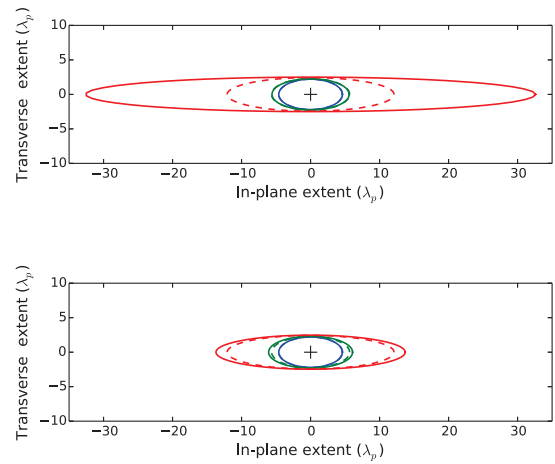


Figure 5: Same as in Figure 3, but for a saddle-type reflector.

previously. Finally, the anisotropic IFZs are larger than the isotropic counterparts, this feature still being more pronounced for positive values of $\epsilon - \delta$.

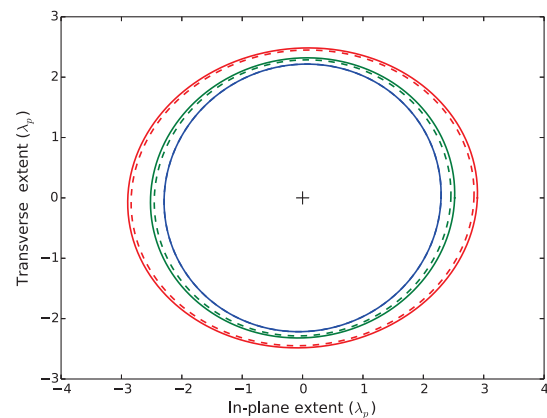
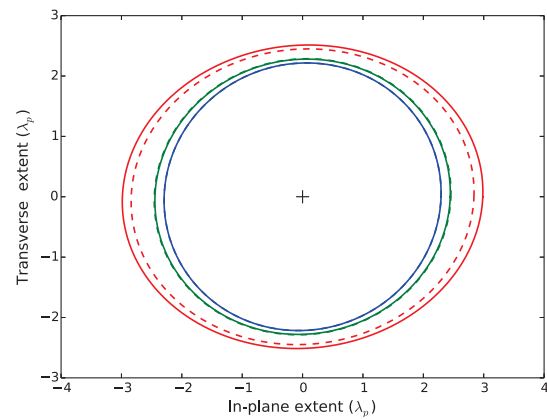


Figure 6: Same as in Figure 3, except that the principal curvature axes of the reflectors do not lie along the Cartesian coordinate axes (rotation by $\phi = 20^\circ$ with respect to the x_1 -axis).

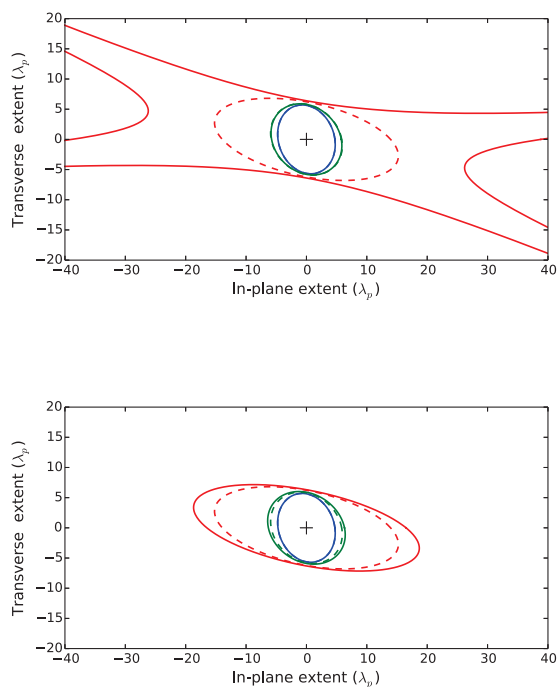


Figure 7: Same as in Figure 4, except that the principal curvature axes of the reflectors do not lie along the Cartesian coordinate axes (rotation by $\phi = 20^\circ$ with respect to the x_1 -axis).

4 Conclusions

The interface Fresnel zone (IFZ) largely contributes to the formation of the reflection and transmission wavefields at an observation point. We have derived analytical expressions, based on approximations of traveltimes, to evaluate its size for converted and non-converted waves reflected or transmitted by a curved reflector between two di-constrained transversely isotropic (DTI) media. Our work thus extends previous studies to the case of oblique wave incidence onto a curved interface of anticline, syncline, and saddle type (with principal curvatures axes not necessarily lying along the Cartesian coordinate axes). We have investigated the shape and size of the IFZ for P-P reflections as a function of anisotropy parameters for various incidence angles and interface curvatures. As in an anisotropic medium the isochron assumes in most cases a non-elliptical shape, the size and shape of the IFZ for reflected waves are known to be predominantly dependent on the curvatures of the isochrons together with the curvatures of the reflector. As expected, the syncline- and the saddle-type reflectors have exhibited very large IFZs compared to those for plane or anticline-type reflectors. In addition, the difference between the anisotropic Thomsen parameters ϵ and δ has been found to also control the shape and size of the IFZ for P-P reflections. The effects are much more pronounced for positive values of the difference $\epsilon - \delta$. The spatial resolution of unmigrated seismic data in anisotropic media will consequently be different from that determined for the same configuration if the media are assumed to be isotropic and/or the reflector plane.

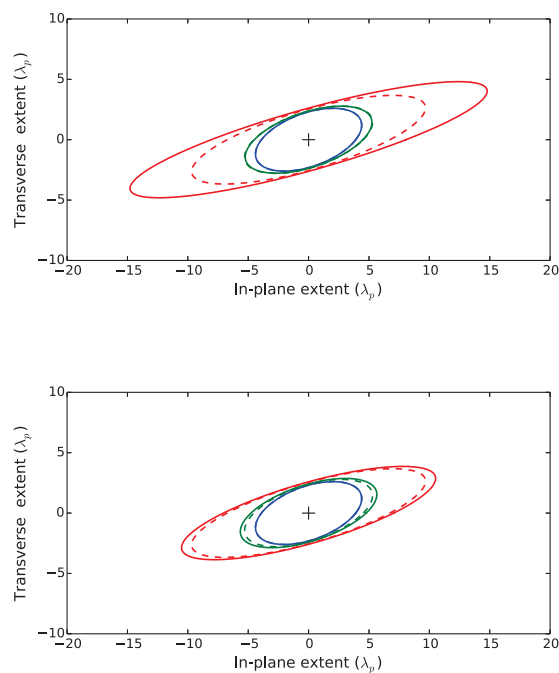


Figure 8: Same as in Figure 5, except that the principal curvature axes of the reflectors do not lie along the Cartesian coordinate axes (rotation by $\phi = 20^\circ$ with respect to the x_1 -axis).

Acknowledgements

We thank the Institute for Engineering and Systems Sciences (INSIS) of the French National Center for Scientific Research (CNRS), the Carnot STAR Institute (ICSTAR), Statoil and the Norwegian Research Council (via the ROSE project) for financial support.

References

- [1] A.A. Asatryan and Yu.A. Kravtsov. Fresnel zones of hyperbolic type from the physical point of view. *Wave Motion*, 10:45–57, 1988.
- [2] V. Červený. *Seismic Ray Theory*. Cambridge University Press, Cambridge UK, 2001.
- [3] C. Chapman. *Fundamentals of seismic wave propagation*. Cambridge University Press, Cambridge UK, 2004.
- [4] D.W.S. Eaton, R.R. Stewart, and M.P. Harrison. The Fresnel zone for P-SV waves. *Geophysics*, 56(3):360–364, 1991.
- [5] N. Favretto-Cristini, P. Cristini, and E. de Bazelaire. Influence on the Interface Fresnel zone on the reflected P-wave amplitude modelling. *Geophysical Journal International*, 171:841–846, 2007.
- [6] N. Favretto-Cristini, P. Cristini, and E. de Bazelaire. Some reflections on reflectors and wave amplitudes. *Acta Acustica*, 93:909–916, 2007.

- [7] N. Favretto-Cristini, P. Cristini, and E. de Bazelaire. What is a seismic reflector like? *Geophysics*, 74(1):T13–T23, 2009.
- [8] E. Iversen. Amplitude, Fresnel zone, and NMO velocity for PP and SS normal-incidence reflections. *Geophysics*, 71(2):W1–W14, 2006.
- [9] J.P. Lindsey. The Fresnel zone and its interpretative significance. *The Leading Edge*, 8(10):33–39, 1989.
- [10] T. J. Moser and V. Červený. Paraxial ray methods for anisotropic inhomogeneous media. *Geophysical Prospecting*, 55:21–37, 2007.
- [11] P.N. Okoye and N.F. Uren. Fresnel zones and spatial resolution for P- and SH-waves in transversely isotropic media. *Geophysics*, 65(4):1168–1178, 2000.
- [12] J. Spetzler and R. Snieder. The Fresnel volume and transmitted waves - a tutorial. *Geophysical Journal International*, 69(3):653–663, 2004.
- [13] O.N. Stavroudis. *The optics of rays, wavefronts, and caustics*. Academic Press, 1972.
- [14] L. Thomsen. Weak elastic anisotropy. *Geophysics*, 51(10):1954–1966, 1986.
- [15] I. Tsvankin. *Seismic signatures and analysis of reflection data in anisotropic media*. Pergamon, 2001.
- [16] Z. Wang. Seismic anisotropy in sedimentary rocks, part 2 : laboratory data. *Geophysics*, 67:1423–1440, 2002.